

Ab initio study of the ideal tensile strength and mechanical stability of transition-metal disilicidesM. Friák,^{1,2} M. Šob,^{1,*} and V. Vitek³¹*Institute of Physics of Materials, Academy of Sciences of the Czech Republic, Žitkova 22, CZ-616 62 Brno, Czech Republic*²*Department of Solid State Physics, Faculty of Science, Masaryk University, Kotlářská 2, CZ-611 37 Brno, Czech Republic*³*Department of Materials Science and Engineering, University of Pennsylvania, 3231 Walnut St., Philadelphia, Pennsylvania 19104-6272, USA*

(Received 9 December 2002; revised manuscript received 24 March 2003; published 3 November 2003)

The ideal tensile test in transition metal disilicides MoSi₂ and WSi₂ with a C11_b structure is simulated by *ab initio* electronic structure calculations using the full-potential linearized augmented plane wave method. The theoretical tensile strength for [001] loading is determined for both disilicides and compared with that of other materials. A full relaxation of all external and one internal structural parameter is performed, and the influence of each relaxation process on energetics and strength of materials studied is investigated. Differences in the behavior of various interatomic bonds including tension-compression asymmetry are analyzed and their origin in connection with the changes of the internal structural parameter is traced. For comparison, the response of bonds in MoSi and CoSi with B2 structure to the [001] loading is also studied.

DOI: 10.1103/PhysRevB.68.184101

PACS number(s): 61.50.Ks, 71.20.Be, 61.66.Dk, 62.20.Dc

I. INTRODUCTION

The strength of plastically deformable materials is usually controlled by the nucleation and motion of dislocations, while in brittle materials fracture habitually initiates at flaws that concentrate stresses. Hence, the theoretical tensile strength, corresponding to the fracture of an ideal, defect free crystal, has rarely been attained. The only materials in which it was approached in the past are whiskers of very pure metals and silicon^{1–5} that are practically dislocation free. However, recent developments in material engineering, such as the production of defect-free thin films and the advancement of various nanostructured materials, have stimulated interest in studies of the ideal strength which in these materials may control both the onset of fracture and the dislocation nucleation, as demonstrated by nanoindentation experiments (see e. g., Refs. 6–10). Theoretically, the ideal strength can be investigated using *ab initio* electronic structure methods based on the density functional theory. First calculations have been made without relaxations of the dimensions of a loaded crystal in the directions perpendicular to the loading axis¹¹ or for unrelaxed shear.^{12,13} Relaxed calculations have been performed for TiC,^{14,15} tungsten,^{16–18} copper,^{19–22} NiAl,^{19,23} aluminum,^{24,20–22} β -SiC,²⁵ diamond,^{26,27} Si,^{27,28} Ge,²⁷ TiN and HfC,¹⁵ iron,^{29–31} Mo and Nb,³² and β -Si₃N₄.³³ Some calculations have been done for nanowires [amorphous Si (Ref. 34) and MoSe nanowires³⁵], grain boundaries^{36–38} and interfaces.³⁹ The calculations of ideal tensile strength for Al,⁴⁰ AlN,^{40,41} β -Si₃N₄,⁴² c-Si₃N₄,⁴³ and an amorphous Si nanowire³⁴ were performed without a relaxation of the dimensions of loaded crystal in the directions perpendicular to the loading axis, i.e., no Poisson contraction was allowed.

In 1997, *ab initio* calculations of theoretical strength under isotropic triaxial (hydrostatic) tension (i.e., negative hydrostatic pressure) also appeared.^{44–49} As the symmetry of the structure does not change during this deformation, simpler *ab initio* approaches may be applied.

Tables summarizing *ab initio* values of theoretical tensile

strengths for various materials are given in Refs. 31 and 50–52, Ref. 51 also includes *ab initio* values of shear strengths and some semiempirical results. An extensive review of semiempirical and *ab initio* calculated values of uniaxial and isotropic triaxial tensile strengths as well as of shear strengths calculated up to 1999 can be found in Ref. 53.

In this paper we investigate the ideal tensile strength of transition-metal (TM) disilicides with C11_b structure, specifically MoSi₂ and WSi₂, by simulating the tensile test of corresponding ideal crystals employing an *ab initio* electronic structure method. A brief account of these results has already been given in Ref. 54. MoSi₂ and WSi₂ are a promising basis for a new generation of high-temperature materials since at these temperatures they combine the ductility and thermal conductivity of metals with high strength, a high melting temperature, corrosion, and a creep resistance of the ceramics.^{55–58} The largest impediment is the low ductility and/or toughness at ambient temperatures when these materials can be loaded close to their ideal strength for some orientations of the loading axes.^{59–65} Thus the onset of dislocation nucleation may be controlled by the ideal strength and its orientation dependence.

During the simulation of the tensile test, complete relaxations of both external and internal parameters are allowed. The theoretical tensile strengths of MoSi₂ and WSi₂ are determined for the [001] loading axis and results are compared with those obtained for other materials. The behavior of interatomic bonds during the tensile loading is analyzed. This analysis reveals two types of TM-Si bonds, “strong” and “weak,” and a tension-compression asymmetry of Si-Si bonds. Since the results for WSi₂ and MoSi₂ are very similar, we only discuss MoSi₂ in detail.

II. METHODOLOGY

Up to now, most of the calculations of the theoretical strength of materials have been based on empirical potentials with their parameters adjusted to experimental data for the

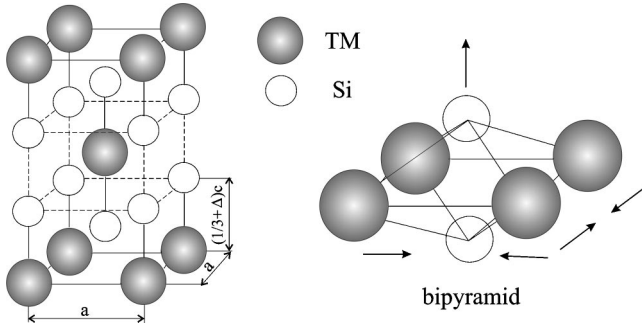


FIG. 1. $C11_b$ structure with the internal parameter Δ defined as a small deviation from the ideal value of $1/3$, and a characteristic substructure, a bipyramid formed by four Mo atoms and two Si atoms. Note that the unit cell of the $C11_b$ structure can also be derived by stacking up three body-centered tetragonal cells along the $[001]$ direction, compressed along the long-period axis (c axis). The central cell exhibiting B2-like occupation is indicated by dashed lines.

equilibrium ground state (for a review see, e.g., Ref. 66 and references therein; ideal shear strengths for all basic cubic structures calculated by means of semiempirical potentials may be found in Ref. 67). However, such empirical approaches may not be valid for materials loaded close to their theoretical strength limits.

In contrast, this is not a problem for *ab initio* electronic structure calculations that start from the fundamental quantum theory. The only input is the atomic numbers of the constituent atoms and, usually, some structural information. This approach is reliable even for highly nonequilibrium states.

In our modeling of the tensile test we start by determining the structure and total energy of the material in the ground state, in our case the $C11_b$ structure (Fig. 1). This is done by finding the total energy as a function of lattice parameters, a and c , and of the internal structural parameter Δ defined in Fig. 1.^{68,69} Then, in the second step, we apply an elongation along the loading axis (in the $[001]$ direction in the present case) by a fixed amount ε_3 that is equivalent to application of a certain tensile stress σ_3 . The $C11_b$ structure is body-centered tetragonal and keeps its tetragonal symmetry during uniaxial loading along the $[001]$ axis; this axis is denoted as 3. For each value of ε_3 , we minimize the total energy by fully relaxing the stresses $\sigma_1 = \sigma_2$ in the directions perpendicular to the axis 3 as well as the internal degree of freedom, Δ . The stress σ_3 is given by

$$\sigma_3 = \frac{2}{c_0 a^2} \frac{dE}{d\varepsilon_3}, \quad (1)$$

where E is the total energy per formula unit [i.e., one transition metal atom and two Si atoms], c_0 is the ground-state value of the lattice parameter in the $[001]$ direction, and a is the lattice parameter in $[100]$ and $[010]$ directions. The inflexion point in the dependence of the total energy on ε_3 corresponds to the maximum of the tensile stress; if some other instability (soft phonon modes, etc.) does not occur

TABLE I. Ground-state lattice parameters of MoSi_2 and WSi_2 .

		a	c	Δ	V_{eq}/V_{expt}
MoSi_2	FLAPW	6.004	14.689	0.0017	0.974
MoSi_2	expt. (Ref. 69)	6.051	14.836	0.0019	1.000
WSi_2	FLAPW	6.020	14.721	0.0013	0.975
WSi_2	expt. (Ref. 69)	6.068	14.870	0.0014	1.000

prior to reaching the inflexion point, it then corresponds to the theoretical tensile strength, σ_{th} .

In this study, we utilized the full-potential linearized augmented plane wave (FLAPW) method.⁷⁰ The electronic structure calculations were performed self-consistently within the local density approximation (LDA).

When simulating the tensile test, crystal lattices are severely distorted and some atoms may move very close together. Therefore, the muffin-tin radii must be sufficiently small to guarantee non-overlapping of the muffin-tin spheres at every stage of the test. We used muffin-tin radii equal to 2.3 a.u. for transition metal atoms and 2.1 a.u. for silicon. These were kept constant in all calculations presented here. The product of muffin-tin radius and the maximum reciprocal space vector, $R_{MT}k_{max}$, was equal to 10, the maximum l value for the waves inside the atomic sphere, l_{max} , and the largest reciprocal vector \mathbf{G} in the Fourier expansion of the charge, G_{max} , were set to 12 and 15, respectively. The number of \mathbf{k} points in the first Brillouin zone was equal to 2000.

III. RESULTS AND DISCUSSION

We first discuss the ground-state properties of MoSi_2 and WSi_2 . The values of the lattice parameters, a and c , the internal parameter, Δ , and the ratio of the calculated equilibrium ground-state and the experimental atomic volume, V_{eq}/V_{expt} , are summarized and compared with the available experimental data⁶⁹ in Table I. The overall agreement is very good; small deviations of lattice parameters (smaller than 1%) are acceptable for the LDA calculations.

In Fig. 2, we display the dependences on ε_3 of (i) the total energy E [Fig. 2(a)], (ii) the internal parameter Δ [Fig. 2(b)], (iii) the tensile stress σ_3 [Fig. 2(c)], (iv) the normalized atomic volume V/V_{eq} [Fig. 2(d)], and (v) lengths of six different types of interatomic bonds between the constituent atoms in MoSi_2 [Fig. 2(e)]; the symbols are explained in the figure caption and in Fig. 2(f). The strain ε_3 for which the tensile stress reaches maximum is clearly seen in Fig. 2(c); it is marked by thin vertical lines in Figs. 2(a)–2(d). The interval of tensile loading is extended so as to include also states beyond the first inflexion point at the energy vs ε_3 curve.

The total energy has a parabolic dependence on ε_3 around the minimum; it then increases with increasing elongation almost linearly in the neighborhood of the first inflexion point [where the tensile stress reaches its maximum—Fig. 2(c)], and then it attains a maximum. Beyond the point $\varepsilon_3 \approx 0.51$, corresponding to a shallow local minimum (this metastable structure is discussed below), the total energy again increases. As it must, the corresponding stress σ_3 van-

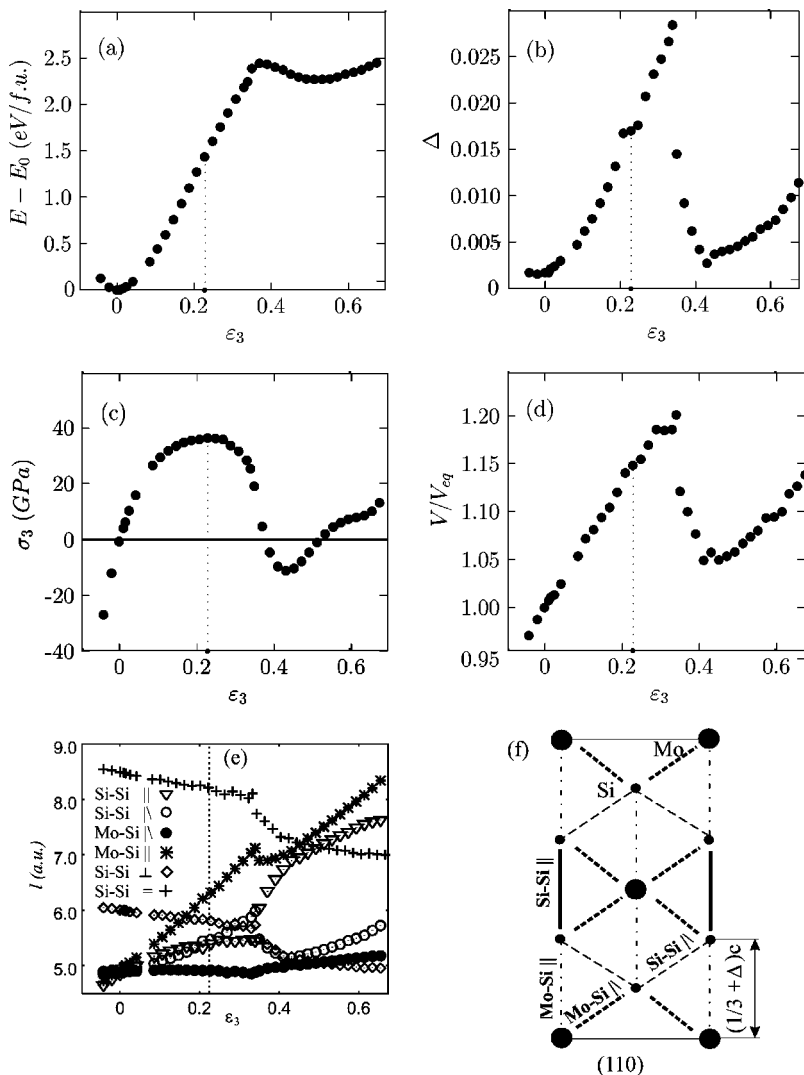


FIG. 2. Variations of the total energy E per formula unit (a), internal parameter Δ (b), tensile stress σ_3 (c), and volume relative to the equilibrium volume V/V_{eq} (d) during the simulation of the tensile test in MoSi_2 . Here E_0 is the ground-state energy and ϵ_3 is the strain in the [001] direction. The position of the inflexion point in the energy dependence and the maximum of the tensile stress are denoted by a thin vertical line. The figure (e) shows the behavior of the length of various atomic bonds during the tensile test; some bonds are identified in (f). The Si atoms are represented by small circles and Mo atoms by large ones. The bond length between the pairs of Mo-Mo and Si-Si atoms in the [100] and [010] directions, corresponding to the lattice parameter perpendicular to the direction of loading, is denoted as $\text{Si-Si} \perp$ [diamonds in (e)], and the bond length between Mo-Mo and Si-Si atoms in the [110] direction is denoted as $\text{Si-Si} =$ [crosses in (e)].

ishes in all three energy extrema (i.e., at the global minimum at the ground state, a local maximum at $\epsilon_3 \approx 0.35$, and a shallow local minimum at $\epsilon_3 \approx 0.51$) and is even negative in the region between the local maximum on the total energy dependence and the metastable structure. Between the inflexion points at $\epsilon_3 \approx 0.22$ and 0.43 , the material is unstable.

The internal parameter Δ [Fig. 2(b)] increases with increasing ϵ_3 , except very close to the ground state where it is almost constant. It reaches its maximum of about 0.030 for $\epsilon_3 \approx 0.35$, which is a relatively high value when compared with the ground state. Then it rapidly decreases and becomes again nearly equal to the ground-state value in the vicinity of the metastable structure. Beyond this point it increases again with increasing elongation. Its full relaxation during the tensile test is vital, as it allows the interatomic bonds to adjust to their proper lengths. The relative atomic volume V/V_{eq} exhibits a behavior very similar to the internal parameter Δ [Fig. 2(d)].

Figure 2(e) shows the dependence of six interatomic bond lengths on ϵ_3 during the tensile test simulation; the numbers of atoms in the first five coordination spheres are given in Table II. Let us first discuss the region accessible, at least in principle, by a tensile test (i.e., prior to reaching the first

inflexion point at the total energy vs ϵ_3 dependence). It was proposed in Ref. 69 that the Mo-Si bonds along the [001] direction [$\text{Mo-Si} \parallel$, asterisks in Fig. 2(e)] are weaker than the Mo-Si bonds in other directions [$\text{Mo-Si} \setminus$, full circles in Fig. 2(e)]. In contrast, it was argued that the Si-Si bonds along the [001] direction [$\text{Si-Si} \parallel$, open triangles in Fig. 2(e)] are stronger than those in other directions [$\text{Si-Si} \setminus$, open circles in Fig. 2(e)]. Our calculations confirm this assertion regarding the Mo-Si bonds. In the $C11_b$ structure, four Mo atoms in the (001) plane form a square of side a which constitutes the basis of a bipyramid completed by two Si atoms above and below the center of this square. It appears that atoms forming these bipyramids try to keep together during extension in the [001] direction (see Fig. 1). That is, the edges of the bipyramid are the $\text{Mo-Si} \setminus$ bonds [full circles in Fig. 2(e)], the length of which is nearly constant during loading, even when the theoretical tensile strength has been exceeded. In agreement with Ref. 69, these bonds can be denoted as “strong” bonds relative to “weak” $\text{Mo-Si} \parallel$ bonds.

The $\text{Si-Si} \parallel$ bonds, defining the height of the bipyramid, elongate under tension [open triangles in Fig. 2(e)] but not as easily as the “weak” $\text{Mo-Si} \parallel$ bonds. This is governed by the relaxation of the internal parameter Δ . In the case of the

TABLE II. Numbers of atoms in the first five coordination spheres in MoSi₂. The rows of the table clearly demonstrate the differences between the coordination of Mo and Si atoms caused by the fact that the coordinates of Mo atoms are fully determined by the symmetry of the body-centered C11_b structure and the internal degree of freedom (parameter Δ) affects only the positions of the Si atoms. As a consequence of more symmetric surroundings of the Mo atoms, the corresponding coordination spheres contain, in general, a higher number of atoms of the same kind than the coordination spheres of the Si atoms. The neighbors of the Si atoms are divided into more numerous and less occupied coordination spheres differing in chemical composition and with diameters slightly modified by the internal parameter Δ . In the case of Si atoms, the information about the number and kind of atoms in the coordination spheres is accompanied by the symbols used in Fig. 2(e) for corresponding interatomic bond lengths.

$-0.04 < \varepsilon_3 < 0$	1 st	2 nd	3 rd	4 th	5 th
Mo	2 Si	8 Si	4 Mo	8 Si	8 Mo
Si	1 Si (∇)	1 Mo (*)	4 Mo (\bullet)	4 Si (\circ)	4 Si (\diamond)
$0 < \varepsilon_3 < 0.15$	1 st	2 nd	3 rd	4 th	5 th
Mo	8 Si	2 Si	4 Mo	8 Si	4 Mo
Si	4 Mo (\bullet)	4 Si (\circ)	1 Si (∇)	1 Mo (*)	4 Si (\diamond)
$0.15 < \varepsilon_3 < 0.18$	1 st	2 nd	3 rd	4 th	5 th
Mo	8 Si	4 Mo	2 Si	4 Mo	8 Si
Si	4 Mo (\bullet)	4 Si (\circ)	1 Si (∇)	4 Si (\diamond)	1 Mo (*)
$0.18 < \varepsilon_3 < 0.29$	1 st	2 nd	3 rd	4 th	5 th
Mo	8 Si	4 Mo	2 Si	4 Mo	8 Si
Si	4 Mo (\bullet)	1 Si (∇)	4 Si (\circ)	4 Si (\diamond)	1 Mo (*)
$0.29 < \varepsilon_3 < 0.35$	1 st	2 nd	3 rd	4 th	5 th
Mo	8 Si	4 Mo	2 Si	4 Mo	8 Si
Si	4 Mo (\bullet)	1 Si (∇)	4 Si (\diamond)	4 Si (\circ)	1 Mo (*)
$0.35 < \varepsilon_3 < 0.51$	1 st	2 nd	3 rd	4 th	5 th
Mo	8 Si	4 Mo	2 Si	4 Mo	8 Si
Si	4 Mo (\bullet)	4 Si (\circ)	4 Si (\diamond)	1 Si (∇)	1 Mo (*)
$0.51 < \varepsilon_3 < 0.66$	1 st	2 nd	3 rd	4 th	5 th
Mo	4 Mo	4 Si	4 Si	4 Mo	2 Si
Si	4 Si (\diamond)	4 Mo (\bullet)	4 Si (\circ)	4 Si (+)	1 Mo (∇)

Si-Si \parallel bonds, their length is influenced by both relaxation processes, i.e., by the decrease of the lattice parameter a [diamonds in Fig. 2(e)] and increase of the internal parameter Δ [Fig. 2(c)]. However, up to $\varepsilon_3 \approx 0.22$, the Si-Si \setminus bonds [open circles in Fig. 2(e)] are extended approximately in the same way as the Si-Si \parallel bonds and, therefore, it is not possible to introduce the notion of “strong” and “weak” Si-Si bonds.

The behavior of Si-Si bonds is somewhat different under compression. The length of the Si-Si \setminus bonds remains nearly constant whereas the length of the Si-Si \parallel bonds changes significantly, similarly as does the length of the Mo-Si \parallel bonds [Fig. 2(e)].

There are also Si-Si and Mo-Mo bonds in the [100] and [010] directions. Their length is equal to the lattice parameter a . They are denoted as Si-Si \perp and marked as open diamonds in Fig. 2(e). In the equilibrium ground state, these bonds are much longer than all the other bonds discussed above. However, during loading their length monotonously decreases. Two regions with a slower decrease can be distinguished [Fig. 2(e)]; they are separated by a region of a more rapid decrease corresponding to the transition between the local maximum and minimum on the total energy vs ε_3 curve. In the metastable state ($\varepsilon_3 \approx 0.51$), the Si-Si \perp and Mo-Mo \perp bonds are the most important since they are the

shortest bonds in this structure.

There are also Si-Si and Mo-Mo bonds in the [110] directions [Fig. 2(e)]. They are denoted as Si-Si $=$ and marked as crosses in Fig. 2(e). Their length is equal to $a\sqrt{2}$. In the neighborhood of the metastable state, their length is essentially the same as the length of the Mo-Si \parallel and Si-Si \parallel bonds.

The tendency of Δ to increase up to $\varepsilon_3 \approx 0.35$ is in agreement with the interpretation of recent experimental tensile test data.⁷¹ The situation in an ideal crystal of WSi₂ is similar to that of MoSi₂.

Figure 3 shows the behavior of Poisson ratio $|\varepsilon_1/\varepsilon_3|$. It oscillates around the value of about 0.16 before reaching the first inflexion point at the dependence of the total energy vs ε_3 . Then, a strong increase in the region corresponding to the rapid change of the lattice parameter a [equal to the length of the Si-Si \perp bonds, Fig. 2(e)] may be observed. It is followed by a slower decrease. For small ε_3 (< 0.05), the numerical errors are bigger than for larger values of ε_3 .

The theoretical tensile strengths, σ_{th} , of MoSi₂ and WSi₂ together with the values for some other materials are summarized in Table III. The strengths as normalized by the Young modulus E_{001} for the [001] loading at low strains, i.e., σ_{th}/E_{001} , are also given. The theoretical tensile strengths for

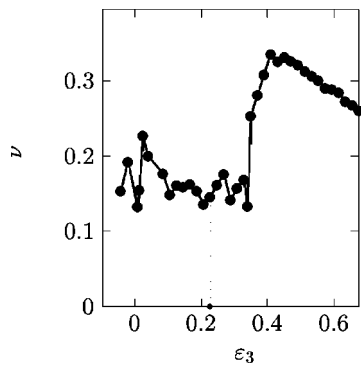


FIG. 3. The behavior of the Poisson ratio during the simulation of the tensile test in MoSi₂.

transition metal disilicides studied (37 and 38 GPa for MoSi₂ and WSi₂, respectively) are comparable with the other values in Table III. Unfortunately, to the best of our knowledge, there are no measurements of ideal tensile strength of MoSi₂ and WSi₂ and, therefore, we are not able to compare our results with experimental data.

It may be seen from Table III that for Fe, Nb, Mo, and W the normalized strengths are not very different from the value of 0.08 which may be expected from the sinusoidal fitting of the energy-strain curve.^{30,51} That is, for the bcc metals, the tensile test corresponds to the relaxed Bain's path connecting the bcc and fcc structures and the parameters of the sinusoid are determined by the Young modulus E_{001} at low strains (curvature) and by the structural energy difference between the relaxed fcc and bcc structures, set at the strain corresponding to the relaxed fcc structure (this structural energy difference is roughly proportional to E_{001} , similarly as the tetragonal shear modulus C' is linearly related to the unrelaxed structural energy difference between the bcc and fcc structures⁷²). The extremum of the total energy for the fcc structure is dictated by the symmetry.^{73,74,16,30} When performing uniaxial tensile deformation along the [001] axis

TABLE III. Theoretical tensile strengths σ_{th} of MoSi₂ and WSi₂ compared with those of other materials. E_{001} is the Young modulus for the [001] loading.

Material	Structure	σ_{th} (GPa)	σ_{th}/E_{001}	Ref.
MoSi ₂	C11 _b	37	0.078	this work
WSi ₂	C11 _b	38	0.079	this work
Fe	A2	12.7	0.089	^{29,31}
		14.2	0.100	³⁰
Nb	A2	13.1	0.079	³²
Mo	A2	28.8	0.078	³²
W	A2	28.9	0.069	¹⁶
		29.5	0.071	¹⁸
Cu	A1	33	0.455	¹⁹
Al	A1	12.1	0.170	²⁴
diamond	A4	225	0.214	²⁶
TiC	B1	44	0.092	¹⁴
NiAl	B2	46	0.527	^{19,23}
β -SiC	B3 (3C)	101	0.321	²⁵

of the other materials shown in Table III, no higher-symmetry structure is encountered along the tensile part of the deformation path and, therefore, it is not surprising that the values of σ_{th}/E_{001} are considerably different from 0.08 in many cases. From this point of view, it is rather astonishing that $\sigma_{th}/E_{001}=0.078$, 0.079, and 0.092 for MoSi₂, WSi₂, and TiC, respectively. In the light of the present knowledge, we consider this fact as an accidental coincidence.

Up to $\varepsilon \sim 0.46$, where the metastable structure occurs, the shortest five interatomic bond lengths are also equal to the radii of corresponding first five coordination spheres of Si atom (also see Table II). Figure 2(e) clearly demonstrates the changes in their dimensions during tensile loading. For instance, for $0 < \varepsilon_3 \leq 0.15$ [see Figs. 2(e) and 2(f)] each Si atom has four Mo atoms in the first coordination sphere, four Si atoms in the second coordination sphere, one Si atom in the third coordination sphere, one Mo atom in the fourth coordination sphere, and four Si atoms in the fifth coordination sphere. At zero deformation, the first four coordination spheres have nearly the same radii. Therefore, we can state that in the ground-state structure each Si atoms has ten nearest neighbors. However, at $\varepsilon_3 \approx 0.15$, four Si atoms in the fifth coordination sphere interchange with one Mo atom in the fourth coordination sphere. Subsequently, at $\varepsilon_3 \approx 0.18$ one Si atom from the third coordination sphere interchanges with four Si atoms from the second sphere. As the loading continues, four Si atoms from the (originally) fifth coordination sphere interchange with those in the (originally) second sphere ($\varepsilon_3 \approx 0.29$). In the vicinity of the local maximum on the total energy dependence, $\varepsilon_3 \approx 0.35$, an abrupt change in the radii of the (originally) second and (originally) third coordination spheres appears. This is again connected with their interchange. Then, in the region of $0.35 \leq \varepsilon_3 \leq 0.43$, the lengths of the Si-Si \backslash and Si-Si \perp (originally the second and fifth coordination spheres) nearly coincide.

The most interesting interchange takes place in the neighborhood of the metastable structure ($\varepsilon_3 = 0.51$), where Si atoms [originally in the fifth coordination sphere, diamonds in Fig. 2(e)] penetrate into the first coordination sphere and the Si atoms from the sixth coordination sphere interchange with the Mo atoms from the (originally) fourth coordination sphere and Si atoms from the (originally) third coordination sphere. Here Mo-Si \backslash bond lengths are equal to the lattice parameter a and the Si-Si \parallel bond lengths are equal to $a\sqrt{2}$ [Fig. 2(e)]. These configurations cannot be reached via tensile loading (as there is a region of instability between the first and second inflexion point on the dependence of the total energy vs ε_3), but may be stabilized in the regions of extended defects such as grain boundaries or dislocations.⁷⁵

The most important difference between the ground-state and metastable structures is found in the bond directions and the coordination numbers. In the ground state, each Si atom has four Si neighbors at $[\pm \frac{1}{2}, \pm \frac{1}{2}, \frac{1}{6} + 2\Delta]$, four Mo neighbors at $[\pm \frac{1}{2}, \pm \frac{1}{2}, -\frac{1}{6} + \Delta]$, one Si neighbor at $[0, 0, -\frac{1}{3} + 2\Delta]$, and one Mo neighbor at $[0, 0, \frac{1}{3} + \Delta]$. The length of these bonds is nearly the same, so that we have ten nearest neighbors, five Si atoms and five Mo atoms. On the other

hand, each Mo atom has in the ground state eight Si neighbors at $[\pm\frac{1}{2}, \pm\frac{1}{2}, \pm(\frac{1}{6}-\Delta)]$ and two Si neighbors at $[0, 0, \pm(\frac{1}{3}+\Delta)]$.

In the metastable structure, each Si atom has the same four Si neighbors $[\pm\frac{1}{2}, \pm\frac{1}{2}, \frac{1}{6}+2\Delta]$ and four Mo neighbors at $[\pm\frac{1}{2}, \pm\frac{1}{2}, -\frac{1}{6}+\Delta]$, but, in addition, also four Si neighbors at $[\pm 1, 0, 0]$ and $[0, \pm 1, 0]$. Mo atoms have, similarly as in the ground-state structure, eight Si neighbors at $[\pm\frac{1}{2}, \pm\frac{1}{2}, \pm(\frac{1}{6}-\Delta)]$, but also four Mo atoms at $[\pm 1, 0, 0]$ and $[0, \pm 1, 0]$. Again, the length of all these bonds is very similar, so that the coordination number in this structure is 12. The neighborhoods of both Si and Mo atoms are essentially fcc-like.

The $C11_b$ unit cell corresponding to the ground-state structure may be considered to be derived by the stacking of three tetragonally compressed bcc-like unit cells along the $[001]$ direction; the bcc-like cell at the center has occupation mimicking the B2 structure (see Fig. 1). During the tensile test simulation these three cells elongate in different ways. When the cell in the middle approaches the ideal B2 cubic lattice dimensions the total energy dependence on ε_3 exhibits a local maximum. The other two cells do not manifest any higher symmetry. The above mentioned connection between the total energy maximum and the symmetry of the central B2-like cell was found only in the case of a fully relaxed tensile test simulation highlighting the nonlinear synergism of both relaxation processes involved. The occurrence of a fcc-like arrangement of atoms corresponding to the local minimum on the dependence of the total energy vs ε_3 (metastable state) is found independently of the relaxations that are allowed. This fact may be crucial for understanding the chemistry of bonds in the materials studied. The difference in the electron density between the ground-state and metastable structure is illustrated in Fig. 4.

Figure 4(a) shows the electron density between the Si atoms in the (001) atomic layer for the ground state, and Fig. 4(b) as for the metastable structure. In the ground state, the Si atoms have the first nearest neighbors in $[331]$ directions and the electron density is concentrated in these directions leading to (with the Si-Si \parallel bond) the local maximum of the electron density in the center among the atoms. In the metastable state, on the other hand, the bond between the Si atoms in the $[001]$ direction is broken and the first nearest neighbors are in the $[100]$ and $[010]$ directions [see the profile of electron density in Fig. 4(b)]. As a result, the electron density has a minimum between the Si atoms.

Another important feature is the fact that the metastable structure does not exhibit a pseudogap at the Fermi level as does the ground-state structure [Figs. 5(a) and 5(b)]. This effect is largely due to the increase of the Mo density of states. The corresponding states make an important contribution to the total energy of the metastable structure.

In all calculations performed till now, we relaxed, for every value of the strain ε_3 , both the perpendicular dimensions of the crystal (or, equivalently, its volume) and the parameter Δ . The relaxation of the internal parameter Δ enables the Si atoms to move in the direction of loading, whereas the atomic positions in the Mo sublattice are dictated only by the

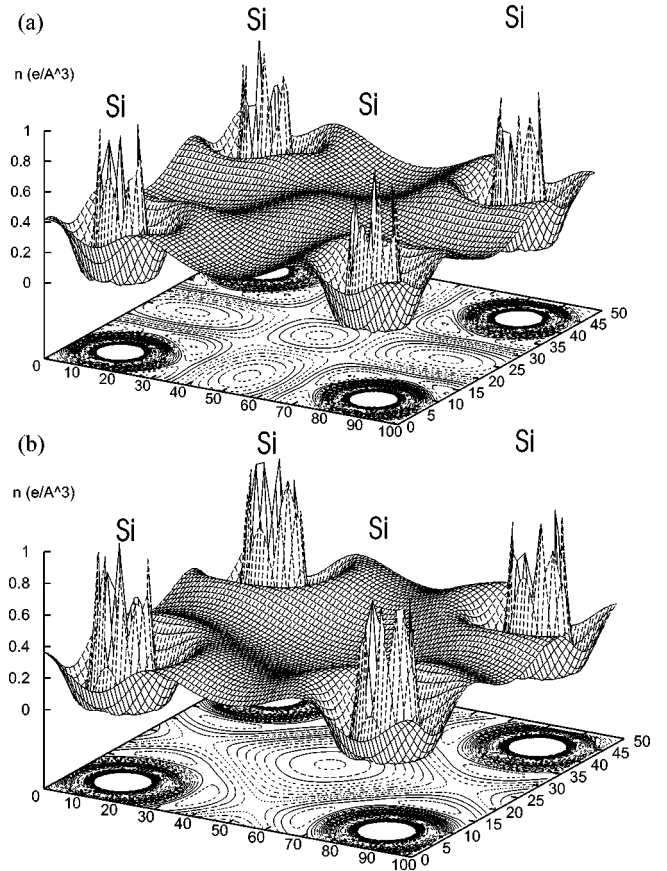


FIG. 4. The electron density in the (001) plane containing Si atoms in the ground state (a) and the metastable state (b). The difference in the shape of electron density around the Si atoms and that in the center among the atoms clearly illustrates the changes in the position of atoms forming the first coordination sphere.

symmetry of the tetragonal body-centered structure. To analyze the influence of various relaxation processes three other variants of the tensile test with loading along the $[001]$ direction and, with the different relaxation processes allowed, have been simulated and compared: (i) both the volume and the internal parameter Δ were kept constant and equal to the values corresponding to the equilibrium ground state ($V/V_{eq} = 1$, $\Delta = 0.0017$), (ii) the volume relaxation was permitted while the internal parameter was kept at $\Delta = 0.0017$, and (iii) the volume was kept constant ($V/V_{eq} = 1$) and the internal parameter Δ was relaxed.

A comparison of the theoretical tensile strength and the position of the first inflexion point obtained for different simulations performed for different relaxation processes is presented in Table IV. As expected, it is seen that the largest strength (at the lowest ε_3) is obtained when no relaxations are allowed, whereas the lowest strength (at the largest ε_3) is found when both the volume and Δ are relaxed. The local maxima on the total energy vs the ε_3 dependence have nearly the same relative energy (with respect to the equilibrium state) but, again, when more relaxation is allowed, they correspond to a larger elongation (Table IV). It may be seen that when relaxations are allowed, the total energy vs the ε_3 dependence is not so steep and the first derivative of the

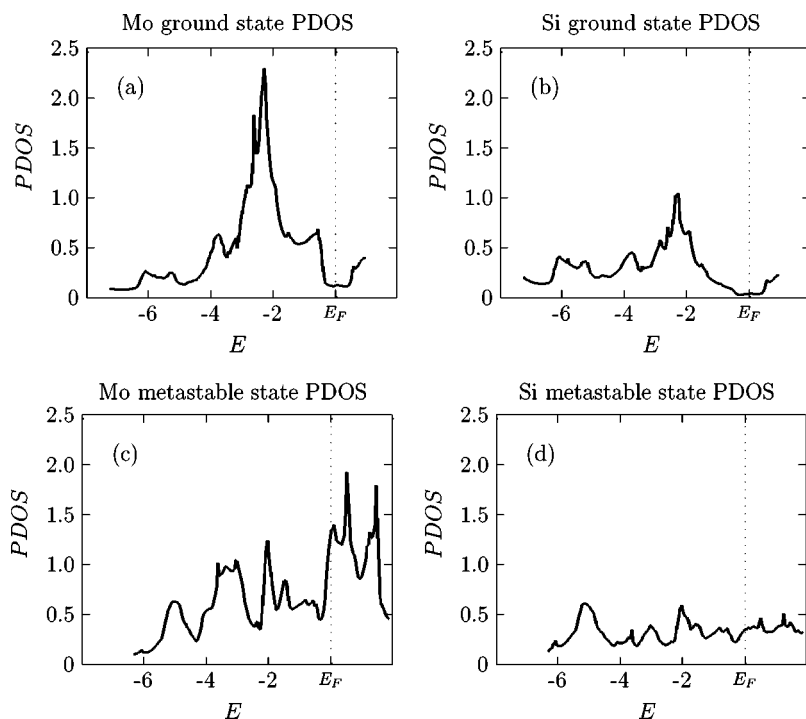


FIG. 5. Variation of density of states for Mo and Si atoms in MoSi_2 with $C11_b$ structure in the ground state [(a) and (b)] and in the metastable structure [(c) and (d)]. The position of the Fermi energy E_F is denoted by a dotted line.

energy with respect to the elongation ε_3 , important for the tensile strength evaluation [see Eq. (1)], is smaller, thus reducing the value of the theoretical tensile strength. Results for WSi_2 are essentially the same as for MoSi_2 .

It is remarkable that the length of the Mo-Si \backslash bond is nearly constant in the whole interval of ε_3 studied (i.e., up to $\varepsilon_3 \approx 0.65$), even if the volume and internal parameter Δ is relaxed [Fig. 2(e)]. To the best of our knowledge, there is only one previous case exhibiting constant bond length as a response to loading. Moroni *et al.*⁷⁶ found that the pseudomorphic phases of FeSi_2 (C1 structure) and CoSi and NiSi (B2 structure) soften dramatically under compressive biaxial strain induced by epitaxy on a (100) substrate. These materials could be deformed from a cube to a tetragonally shaped body (up to 10% in the basal plane) without any cost of energy. This supersoft effect is reflected by zero strain energy, constant volume, constant bond energies (defined in Ref. 76) as well as a constant TM-Si bond strength and length during the deformation. As the volume of the material during such deformation is nearly constant, the material may be regarded as an ideal incompressible liquid. As the atoms of the central bcc-like cell in the $C11_b$ structure have the

same positions as in B2 structure compressed in the [001] direction, it may be instructive to investigate the tetragonal deformation of CoSi and MoSi in the B2 structure.

In Fig. 6, we display the total energy of CoSi [Fig. 6(a)] and MoSi [Fig. 6(b)] in a high-symmetry crystal structure B2 as a function of elongation ε_3 during the simulation of the tensile loading in [001] direction. The corresponding bond-lengths are shown in Figs. 6(c) (CoSi) and 6(d) for MoSi.

The TM-Si bond, oriented along the [111] direction in the B2 structure, corresponds (also with respect to the direction of loading) to the strong Mo-Si \backslash bond in the [331] direction in MoSi_2 with a $C11_b$ structure. Also its length in the B2 structure [$l \in (4.92, 4.96)$ a.u.] is very similar to the length of the strong Mo-Si \backslash bond in MoSi_2 with the length $l \in (4.88, 4.95)$ a.u. A very similar constant behavior of TM-Si bond in B2 structure was found for both CoSi and MoSi [see Figs. 6(c) and 6(d)]. In contrast to this qualitative agreement in the bond-length behavior the nearly constant total energy profile in wide range of deformation was observed only in the case of CoSi.

A nearly constant volume was found for CoSi (but not for MoSi) in quite broad range of deformation $\varepsilon_3 \in$

TABLE IV. Theoretical tensile strength σ_{th} for MoSi_2 , the positions of the first inflexion point ε_3^{th} and the first maximum ε_3^{max} at the total energy vs the ε_3 dependence for different relaxation processes. The total energy differences between the first energy maximum and ground state ($E^{max} - E_0$) per formula unit (f.u.) are also given.

Relaxation	None	Δ	V/V_{eq}	$V/V_{eq} + \Delta$
σ_{th} (GPa)	54	53	43	37
ε_3^{th}	0.17 ± 0.02	0.17 ± 0.02	0.20 ± 0.04	0.22 ± 0.04
$E^{max} - E_0$ (eV/f.u.)	2.46	2.45	2.45	2.44
ε_3^{max}	0.33	0.33	0.36	0.37

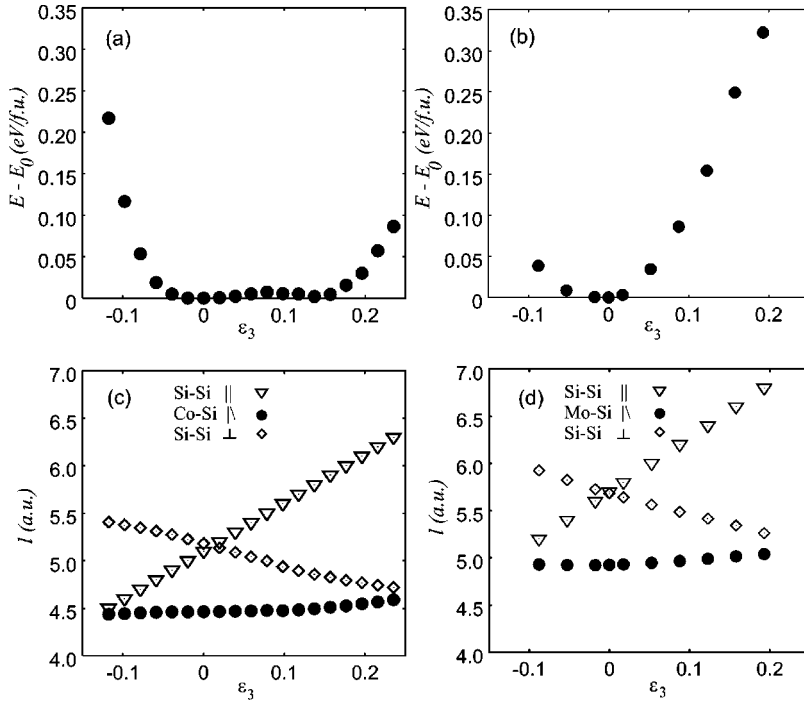


FIG. 6. Variation of the total energy E per formula unit measured with respect to the equilibrium total energy of the B2 phase E_0 during the tensile test simulation in CoSi (a) and MoSi (b) as a function of ϵ_3 . (c) and (d) show the behavior of the length of three atomic bonds within the B2 structure for CoSi (c) and MoSi (d).

($-0.05, 0.14$). As a consequence, the Poisson ratio reaches an extremely high value equal to $\nu = 0.485$ ($1/2$ corresponds to exactly constant volume). In the case of MoSi the value of 0.41 lies close to the upper limit of the range 0.28 – 0.42 typical for most materials.

During the tensile test simulation in MoSi₂, the central tetragonally deformed B2-like cell (Fig. 1), compressed in the $[001]$ direction in the ground state, reaches exactly the B2 proportions at $\epsilon_3 \approx 0.35$ corresponding to the local maximum of the total energy [see Fig. 2(a)]. In contrast to this, in the case of MoSi, the B2 (CsCl) structure represents the

ground state and the total energy of MoSi as a function of tetragonal deformation exhibits a minimum for the B2 configuration.

The density of states at the Fermi level shows a local maximum for the equilibrium B2 structure for both CoSi and MoSi [see Figs. 7(c) and 7(d)]. For CoSi another maximum was found for the elongation of $\epsilon_3 \approx 0.10$, close to the states corresponding to a local maximum for both the total energy [Fig. 6(a)] and volume [Fig. 7(a)].

From the above comparison one may conclude that the origin of the constant TM-Si bond-length discussed above in

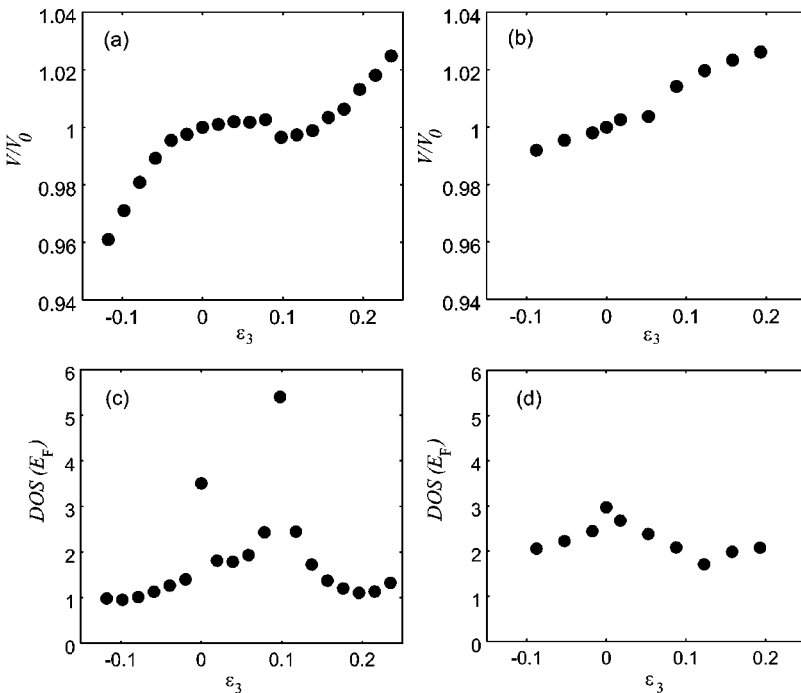


FIG. 7. Variation of volume V measured with respect to the equilibrium volume of the B2 phase V_0 during the tensile test simulation in CoSi (a) and MoSi (b) as a function of ϵ_3 . (c) and (d) show for the corresponding dependence of the density of states (DOS) at the Fermi energy E_F of materials studied with B2 structure [CoSi (c) and MoSi (d)].

MoSi, MoSi₂, and CoSi may be dependent on the crystal structure and the TM constituent. The main qualitative difference is that the constant bond length in the case of MoSi and MoSi₂ is not accompanied by a nearly constant total energy profile and, consequently, by supersoft properties.

IV. CONCLUSIONS

We simulated the tensile test in ideal crystals of MoSi₂ and WSi₂ loaded along the [001] axis by using first-principles full potential electronic structure calculations. These calculations demonstrate a similarity in the behavior of the materials studied. We determined the values of theoretical tensile strengths of the materials studied and compared them with those obtained theoretically for other materials. The effect of two different relaxation processes on the total energy and interatomic bonds was studied in detail and a metastable state was found. The analysis of bond lengths variation under uniaxial stress shows that it is possible to distinguish “strong” and “weak” TM-Si bonds. The behavior of Si-Si bonds is more complex and exhibits a tension-compression asymmetry connected with the relaxation of the internal parameter of C11_b structure that favors a cooperative movement of Si atoms.

For comparison, the response of bonds to the [001] loading in MoSi and CoSi with B2 (CsCl) structure was also studied. The behavior of TM-Si bonds in these materials, though qualitatively similar as in MoSi₂ and WSi₂, is in the case of CoSi accompanied by a nearly constant total energy during the [001] loading. This supersoft behavior, reported up to now for biaxial strains in some TM silicides,⁷⁶ was found here under uniaxial loading conditions. Our results suggest that the origin of the nearly constant TM-Si bond length discussed in this paper may be specific to each material.

ACKNOWLEDGMENTS

This research was supported by the Grant Agency of the Czech Republic (Project No. 202/03/1351), the Grant Agency of the Academy of Sciences of the Czech Republic (Project No. IAA1041302), and by the U.S. Department of Energy, Basic Energy Sciences (Grant No. DE-FG02-98ER45702). A part of this study has been performed in the framework of the COST Project No. OC 523.90. The use of the computer facility at the MetaCenter of the Masaryk University, Brno, and at the Boston University Scientific Computing and Visualization Center is acknowledged.

*Corresponding author. Email address: mojmir@ipm.cz.

¹S.S. Brenner, J. Appl. Phys. **27**, 1484 (1956).

²S.S. Brenner, J. Appl. Phys. **28**, 1023 (1957).

³R.V. Coleman, B. Price, and N. Cabrera, J. Appl. Phys. **28**, 1360 (1957).

⁴G.L. Pearson, W.T. Read, Jr., and W.L. Feldmann, Acta Metall. **5**, 181 (1957).

⁵E.M. Nadgornyi, Usp. Fiz. Nauk **77**, 201 (1962) [Sov. Phys. Usp. **5**, 462 (1962)].

⁶R.P. Vinci and J.J. Vlassak, Annu. Rev. Mater. Sci. **26**, 431 (1996).

⁷D.F. Bahr, D.E. Kramer, and W.W. Gerberich, Acta Mater. **46**, 3605 (1998).

⁸A. Gouldstone, H.J. Koh, K.Y. Zeng, A.E. Giannakopoulos, and S. Suresh, Acta Mater. **48**, 2277 (2000).

⁹C.L. Woodcock and D.F. Bahr, Scr. Mater. **43**, 783 (2000).

¹⁰O.R. de la Fuente, J.A. Zimmerman, M.A. Gonzalez, J. de la Figuera, J.C. Hamilton, W.W. Pai, and J.M. Rojo, Phys. Rev. Lett. **88**, 036101 (2002).

¹¹E. Esposito, A.E. Carlsson, D.D. Ling, H. Ehrenreich, and D.C. Gelatt, Jr., Philos. Mag. **41**, 251 (1980).

¹²A.T. Paxton, P. Gumbsch, and M. Methfessel, Philos. Mag. Lett. **63**, 267 (1991).

¹³W. Xu and J.A. Moriarty, Phys. Rev. B **54**, 6941 (1996).

¹⁴D.L. Price, B.R. Cooper, and J.M. Wills, Phys. Rev. B **46**, 11 368 (1992).

¹⁵S.-H. Jhi, S.G. Louie, M.L. Cohen, and J.W. Morris, Jr., Phys. Rev. Lett. **87**, 075503 (2001).

¹⁶M. Šob, L.G. Wang, and V. Vitek, Mater. Sci. Eng., A **234-236**, 1075 (1997).

¹⁷C.R. Krenn, D. Roundy, J.W. Morris, Jr., and M.L. Cohen, Mater. Sci. Eng., A **319-321**, 111 (2001).

¹⁸D. Roundy, C.R. Krenn, M.L. Cohen, and J.W. Morris, Jr., Philos. Mag. A **81**, 1725 (2001).

¹⁹M. Šob, L.G. Wang, and V. Vitek, Kovove Mater. **36**, 145 (1998).

²⁰D. Roundy, C.R. Krenn, M.L. Cohen, and J.M. Morris, Jr., Phys. Rev. Lett. **82**, 2713 (1999).

²¹C.R. Krenn, D. Roundy, J.W. Morris, Jr., and M.L. Cohen, Mater. Sci. Eng., A **317**, 44 (2001).

²²S. Ogata, J. Li, and S. Yip, Science **298**, 807 (2002).

²³M. Šob, L.G. Wang, and V. Vitek, Philos. Mag. B **78**, 653 (1998).

²⁴W. Li and T. Wang, J. Phys.: Condens. Matter **10**, 9889 (1998).

²⁵W. Li and T. Wang, Phys. Rev. B **59**, 3993 (1999).

²⁶R.H. Telling, C.J. Pickard, M.C. Payne, and J.E. Field, Phys. Rev. Lett. **84**, 5160 (2000).

²⁷D. Roundy and M.L. Cohen, Phys. Rev. B **64**, 212103 (2001).

²⁸Y. Umeno and T. Kitamura, Mater. Sci. Eng., B **88**, 79 (2002).

²⁹M. Friák, M. Šob, and V. Vitek, in *Proc. Int. Conf. JUNIOR-MAT'01* (Faculty of Mechanical Engineering, Brno University of Technology, Brno, 2001), p. 117.

³⁰D.M. Clatterbuck, D.C. Chrzan, and J.W. Morris, Jr., Philos. Mag. Lett. **82**, 141 (2002).

³¹M. Friák, M. Šob, and V. Vitek, Philos. Mag. (2003, in press).

³²W. Luo, D. Roundy, M.L. Cohen, and J.W. Morris, Jr., Phys. Rev. B **66**, 094110 (2002).

³³S. Ogata, N. Hirotsaki, C. Kocer, and Y. Shibutani, J. Mater. Res. **18**, 1168 (2003).

³⁴G. Galli, F. Gygi, and A. Catellani, Phys. Rev. Lett. **82**, 3476 (1999).

³⁵F.J. Ribeiro, D.J. Roundy, and M.L. Cohen, Phys. Rev. B **65**, 153401 (2002).

³⁶M. Kohyama, Mater. Sci. Forum **294-296**, 657 (1999).

³⁷J.C. Hamilton and S.M. Foiles, Phys. Rev. B **65**, 064104 (2002).

³⁸M. Kohyama, Phys. Rev. B **65**, 184107 (2002).

- ³⁹I.G. Batirev, A. Alavi, M.W. Finnis, and T. Deutsch, *Phys. Rev. Lett.* **82**, 1510 (1999).
- ⁴⁰S. Ogata and H. Kitagawa, *Comput. Phys. Commun.* **15**, 435 (1999).
- ⁴¹H. Kitagawa and S. Ogata, *Key Eng. Mater.* **161-163**, 443 (1999).
- ⁴²S. Ogata, N. Hirotsaki, C. Kocer, and H. Kitagawa, *Phys. Rev. B* **64**, 172102 (2001).
- ⁴³C. Kocer, N. Hirotsaki, and S. Ogata, *Phys. Rev. B* **67**, 035210 (2003).
- ⁴⁴P. Šandera, J. Pokluda, L.G. Wang, and M. Šob, *Mater. Sci. Eng., A* **234-236**, 370 (1997).
- ⁴⁵Y. Song, R. Yang, D. Li, W.T. Wu, and Z.X. Guo, *Phys. Rev. B* **59**, 14 220 (1999).
- ⁴⁶M. Černý, P. Šandera, and J. Pokluda, *Czech. J. Phys.* **49**, 1495 (1999).
- ⁴⁷Y. Song, R. Yang, D. Li, and Z.X. Guo, *Philos. Mag. A* **81**, 321 (2001).
- ⁴⁸Y. Song, Z.X. Guo, and R. Yang, *Philos. Mag. A* **82**, 1345 (2002).
- ⁴⁹M. Černý, J. Pokluda, P. Šandera, M. Friák, and M. Šob, *Phys. Rev. B* **67**, 035116 (2003).
- ⁵⁰M. Šob, L.G. Wang, M. Friák, and V. Vitek, in *Computational Modeling of Materials, Minerals, and Metals Processing*, edited by M. Cross, J.W. Evans, and C. Bailey (The Minerals, Metals & Materials Society, Warrendale, PA, 2001), p. 715.
- ⁵¹J.W. Morris, Jr., C.R. Krenn, D. Roundy, and M.L. Cohen, in *Phase Transformations and Evolution in Materials*, edited by P.E.A. Turchi and A. Gonis (The Minerals, Metals & Materials Society, Warrendale, PA, 2000), p. 187.
- ⁵²M. Šob, M. Friák, D. Legut, and V. Vitek, in *Proc. 3rd Int. Alloy Conf.: An Interdisciplinary Approach to the Science of Alloys in Metals, Minerals and Other Materials Systems, Estoril/Cascais, Portugal, June 30-July 5, 2002*, edited by P.E.A. Turchi and A. Gonis (Kluwer, Boston-Dordrecht-London, 2003, in press).
- ⁵³J. Pokluda and P. Šandera, in *METAL 2000 (Proc. 9th Int. Metallurgical Conf., Ostrava, Czech Republic, May 16-18, 2000)*, edited by T. Prnka (Tanger, Ostrava, 2000).
- ⁵⁴M. Friák, M. Šob, and V. Vitek, in *High-Temperature Ordered Intermetallic Alloys IX*, edited by J.H. Schneibel, K.J. Hemker, R.D. Noebe, S. Hanada, and G. Sauthoff, MRS Symposium Proceeding No. 646 (Materials Research Society, Warrendale, PA, 2001), paper N4.8.
- ⁵⁵J. Petrovic and A.K. Vasudevan, *Mater. Sci. Eng., A* **261**, 1 (1999).
- ⁵⁶J.J. Petrovic, *Intermetallics* **8**, 1175 (2000).
- ⁵⁷M. Yamaguchi, H. Inui, and K. Ito, *Acta Mater.* **48**, 307 (2000).
- ⁵⁸N.S. Stoloff, C.T. Liu, and S.C. Deevi, *Intermetallics* **8**, 1313 (2000).
- ⁵⁹K. Ito, H. Inui, Y. Shirai, and M. Yamaguchi, *Philos. Mag. A* **72**, 1075 (1995).
- ⁶⁰K. Ito, T. Yano, T. Nakamoto, H. Inui, and M. Yamaguchi, *Intermetallics* **4**, S119 (1996).
- ⁶¹K. Ito, T. Yano, T. Nakamoto, M. Moriwaki, H. Inui, and M. Yamaguchi, *Prog. Mater. Sci.* **42**, 193 (1997).
- ⁶²A. Newman, T. Jewett, S. Sampath, C. Berndt, and H. Herman, *J. Mater. Res.* **13**, 2662 (1998).
- ⁶³H. Inui, T. Nakamoto, K. Ishikawa, and M. Yamaguchi, *Mater. Sci. Eng., A* **261**, 131 (1999).
- ⁶⁴U. Messerschmidt, S. Guder, L. Junker, M. Bartsch, and M. Yamaguchi, *Mater. Sci. Eng., A* **319**, 342 (2001).
- ⁶⁵L. Junker, M. Bartsch, and U. Messerschmidt, *Mater. Sci. Eng., A* **328**, 181 (2002).
- ⁶⁶F. Milstein and S. Chantasiriwan, *Phys. Rev. B* **58**, 6006 (1998).
- ⁶⁷P. Šandera and J. Pokluda, *Scr. Metall. Mater.* **29**, 1445 (1993).
- ⁶⁸L.F. Mattheiss, *Phys. Rev. B* **45**, 3252 (1992).
- ⁶⁹K. Tanaka, K. Nawata, K. Yamamoto, H. Inui, M. Yamaguchi, and M. Koiwa, in *Proceedings of the U.S.-Japan Workshop on Very High Temperature Structural Materials*, edited by T. Pollock and M. Yamaguchi (Carnegie Mellon University, Pittsburgh, PA, 1999), pp. 61–66.
- ⁷⁰P. Blaha, K. Schwarz, and J. Luitz, WIEN97, Technical University of Vienna, 1997 (improved and updated Unix version of the original copyrighted WIEN code), edited by P. Blaha, K. Schwarz, P. Sorantin, and S.B. Trickey [*Comput. Phys. Commun.* **59**, 399 (1990)].
- ⁷¹K. Tanaka, K. Nawata, H. Inui, M. Yamaguchi, and M. Koiwa, in *High-Temperature Intermetallic Alloys IX* (Ref. 54), paper N4.3.
- ⁷²J.M. Wills, O. Eriksson, P. Söderlind, and A.M. Boring, *Phys. Rev. Lett.* **68**, 2802 (1992).
- ⁷³P.J. Craievich, M. Weinert, J.M. Sanchez, and R.E. Watson, *Phys. Rev. Lett.* **72**, 3076 (1994).
- ⁷⁴M. Šob, L.G. Wang, and V. Vitek, *Comp. Mat. Phys.* **8**, 100 (1997).
- ⁷⁵C. Schmidt, F. Ernst, M.W. Finnis, and V. Vitek, *Phys. Rev. Lett.* **75**, 2160 (1995).
- ⁷⁶E.G. Moroni, R. Podlucky, and J. Hafner, *Phys. Rev. Lett.* **81**, 1969 (1998).